IOPscience iopscience.iop.org

Home Search Collections Journals About Contact us My IOPscience

Direct image-based fractal characterization of morphologies and structures of wax crystals in waxy crude oils

This article has been downloaded from IOPscience. Please scroll down to see the full text article.

2006 J. Phys.: Condens. Matter 18 11487

(http://iopscience.iop.org/0953-8984/18/50/006)

View the table of contents for this issue, or go to the journal homepage for more

Download details:
IP Address: 129.252.86.83
The article was downloaded on 28/05/2010 at 14:52

Please note that terms and conditions apply.

INSTITUTE OF PHYSICS PUBLISHING JOURNAL OF PHYSICS: CONDENSED MATTER

J. Phys.: Condens. Matter **18** (2006) 11487–11506 doi:10.1088/0953-8984/18/50/006

Direct image-based fractal characterization of morphologies and structures of wax crystals in waxy crude oils

Peng Gao, Jinjun Zhang and Guixia Ma

MOE Key Laboratory of Petroleum Engineering (Beijing Key Laboratory of Urban Oil & Gas Distribution Technology), China University of Petroleum (Beijing), Beijing Changping 102249, People's Republic of China

E-mail: gaopengmail@126.com

Received 9 August 2006, in final form 23 October 2006
Published 27 November 2006
Online at stacks.iop.org/JPhysCM/18/11487

Abstract

The morphology and structure of wax crystals are among the factors dominating rheological characteristics of a waxy crude oil at temperatures below the wax appearance temperature (WAT). In several reported researches fractal dimensions were employed in describing the waxy crude oil microstructures; however, they were all determined via the indirect approach, i.e. deduced from the rheological data. This paper presents a direct fractal characterization approach based on micrographs of wax crystals. The box-counting method is applied to the wax crystal images of three waxy crude oils beneficiated with and without pour-point-depressants (PPDs), and for the fractal measurements the t-distribution tests of hypothesis on linear regression are performed at the significance level of 0.01. It is demonstrated that the boundary fractal dimensions from micrographs of different visual fields of a specimen are almost identical, with the maximum and minimum relative ranges being 9.97% and 1.88% respectively, and with the standard deviation ranging from 0.0549 to 0.0107. Then the wax crystal structures are determined as fractal at the confidence level of 99%. All the listed absolute t-statistics with the minimum of 29.568 are much higher than the corresponding t-quantiles with the maximum of 3.4995. The results also show that the larger value of the boundary box dimension represents the higher complexity and irregularity of the wax crystal morphology. The box dimension increases with decreasing oil temperature for each waxy crude oil. After the oil is beneficiated with a PPD, the box dimension increases at each given temperature. Thus, it is feasible to use fractal dimensions to characterize the waxy crude oil microstructures. This helps to probe the rheology–microstructure relation.

 © 2006 IOP Publishing Ltd Printed in the UK

1. Introduction

The rheology of waxy crude oils is influenced greatly by their complex primary components such as wax, resin and asphaltene [1–6], as well as by external factors including thermal and shear history [7–10]. At temperatures below the wax appearance temperature (WAT), the precipitated wax amount and the morphology and structure of wax crystals are predominant factors causing the rheological behaviours of waxy crude oils to be complex to a large extent. Actually, it is by modifying the morphology and structure of wax crystals that the thermal and shear history affect the flow properties of waxy crude oils. This principle has been applied to some beneficiation processes for pipelining waxy crude oils, e.g. heat treatment and pour-point-depressant (PPD) beneficiation. Here, a PPD is a chemical additive that can improve the flow properties of waxy crude oils, e.g. reducing the pour point and viscosity.

However, due to the high complexity and irregularity of wax crystal structures, their quantitative characterization is hard to achieve. This has hampered further study on the rheology–microstructure relationship.

On the subject of quantifying waxy crystal morphology, the grain size, the shape features of wax crystals, and the continuous liquid phase features from waxy crude oil micrographs were extracted through 15 statistical parameters in [11, 12]. With this method, the quantitative description of wax crystal morphology in detail was accomplished. But it involves too many description parameters. Moreover, the method is insensitive to the overall nonlinearity of the wax crystal microstructures.

Fractal dimensions have been employed in describing microstructures of waxy crude oils in several published researches. After having examined the micrographs reported in [13–16], Visintin *et al* [10] suggested that the wax crystalline masses could be classified as fractal. However, few substantial investigations combining with the fractal characterization were involved in [10]. Lorge and Djabourov [17] assumed that the wax crystal clusters had a fractal structure and developed a simple relation between the suspension viscosity η and the shear rate $\dot{\gamma}$:

$$\frac{\eta - \eta_0}{\eta_0} \sim \psi \left(\frac{\eta_0 \dot{\gamma} a^3}{\Gamma_c} \right)^{(D-3)/3} \tag{1}$$

where η_0 is the solvent viscosity; ψ is the volume fraction of particles; a is the radius of a particle supposed to be spherical; Γ_c is the critical bending torque; and D is the fractal dimension of the cluster structure. However, this simple analysis is rigorously valid only for very dilute suspensions and few data are provided for verification.

Lopes da Silva and Coutinho [18] also assumed the wax aggregates as fractal. Then via the scaling theory in the framework of colloidal suspension, and referring to some findings [19–21], they deduced the fractal dimensions for three cured wax-oil gels in terms of

$$G' = \lambda \phi^{\beta/(d-d_f)} \tag{2}$$

where G' is the elastic modulus; ϕ is the particle volume fraction; d is the Euclidean dimension of the system; d_f is the fractal dimension of the flocs; β is a constant. The fractal dimensions for three waxy oils were calculated, being 1.7, 1.9 and 2.2 respectively. However, (2) did not take some essential factors into account, such as the fractal dimension–temperature relation, and the composition of a waxy crude oil.

Similarly, by using the gel storage modulus model developed by Uriev *et al* [22] in the colloidal gels with fractal structure,

$$G' \sim k G_p C^{(3+D_s)/(3-D)}, \tag{3}$$

Kané *et al* [9] analysed the relation between the shear moduli and the crystal content of the crude oil gels cooled in static conditions. The coefficient k takes the contact zone between the

Table 1. Physical properties and some experimental conditions of waxy crude oils.

Parameter	Test method	Oil A	Oil B	Oil C
Pour point (°C)	ASTM D97-2004	15	15	35
Wax appearance temperature (°C)	By DSC measurement	25	24	49
Wax content (wt%)	By DSC measurement	10.4	11.2	20.8
Resin and asphaltene content (wt%)	IP 143/96	5.93	3.19	10.4
Heat treatment temperature (°C)	—	55	50	65
PPD dosage (mg kg^{-1})	—	50	50	200
Pour point of PPD-beneficiated oil (°C)	ASTM D97-2004	5	1	25

particles into account and G_p is the shear modulus of the single particles. C is the particle concentration. D is the fractal dimension of an aggregate, and D_s is the fractal dimension of the mesh backbone. Kané *et al* [9] pointed out that the key parameters which governed the viscoelastic moduli may be related to the molecular compositions of the oils and some morphological differences of the crystals. And the relations were still a little ambiguous [9].

For waxy crude oil gels under shearing and in the framework of the colloidal suspensions, Kané *et al* [9] combined the Krieger–Dougherty model [23] with some relations defined by [24] and [25], and then obtained the following equation:

$$\eta = \eta_s \left[1 - \frac{\psi}{\phi_m} \left(\frac{\sigma}{\sigma_c} \right)^{-(3-D)/3} \right]^{-[\eta]\phi_m} \tag{4}$$

where η_s is the solvent viscosity; ψ is the real volume fraction of primary particles; σ is the shear stress; σ_c is the cohesion stress; $[\eta]$ is the intrinsic viscosity of the particles and ϕ_m is the maximum volume fraction for packing. Thus, the fractal dimension D was introduced into the model. For each temperature, the fractal dimension was assumed constant and it can be fitted using the viscosity data.

Fractal dimensions have been used in describing the microstructures of waxy crude oils in the above-mentioned literature [9, 17, 18]; however, according to some equations of colloidal suspensions, their fractal dimension values were deduced from the rheological data. These approaches could be ascribed to indirect characterization [26]. On the contrary, in this work the direct fractal characterization approach [26] is adopted based on the microscopic images of wax crystals. With this approach, the microstructure data can be obtained independently. The microscopic and rheological experiments on three waxy crude oils beneficiated with and without pour-point-depressants (PPDs) were performed. Subsequently the box-counting method was applied and its measurement reliability was evaluated using the t-distribution test of hypothesis on linear regression at the significance level of 0.01. The results show that the morphology and structure of wax crystals can be effectively characterized as a whole via the fractal dimension.

2. Materials and methods

2.1. Specimen preparation and handling

In order to acquire typical microscopic images of wax crystals, three waxy crude oils from different oil fields were chosen. For better repeatability of viscosity measurement, the thermal and shearing history of the virgin crude oil specimens were removed by heating the specimens to 80 °C for 2 h and then leaving them cool statically. The specimens were then kept at room temperature for at least 48 h before being used in experiments. Their basic physical properties are given in table 1.

The investigation proceeded as follows. First, the oil specimen was preheated to the corresponding heat treatment temperature (table 1) to completely melt all the existing wax. After heat treatment for 25 min, the oil was cooled to the filling temperature at the cooling rate of 1.0 °C min^{-1} and held isothermally for 15 min. Then the specimen was divided into two parts, one for rheological measurement and the other for optical microscopy examination. More details are presented in the following sections.

In the procedure, the filling temperature was generally 3 °C above the WAT, and designed for avoiding the resulting evaporation loss if the oil specimen was loaded into the rheometer cup too early. To precisely explore relations between the rheology or flow properties and microstructures, the oil specimens should be sealed in the same vessel and experience the same thermal and shear history before the macro-property measurements and optical microscopy examination. In addition, the PPDs used for modifying the flow behaviours of crude oils are experimental chemical additives.

2.2. Differential scanning calorimetry (DSC)

All thermal analyses were performed using a TA2000/MDSC2910 DSC apparatus (TA Instruments, USA). More calibration and measurement details are showed in [27]. According to an empirical linear correlation with the DSC total thermal effect Q, the wax content of a crude oil can be easily determined [27].

2.3. Gel point/pour point

The gel point of the crude oil was determined according to the Chinese Standard Petroleum Test Method (SY/T 0541-94). The oil specimen was heated to the heat treatment temperature (table 1), transferred to the gel-point glass test-tube preheated at the same temperature, and then cooled at a rate of 0.5 °C min^{-1}. The specimen flowability was checked every 2 °C from 8 °C above the expected gel-point temperature. The gel point was the highest temperature at which specimen movement could not be observed when the tube was held horizontally for 5 s. Its repeatability is ±2 °C.

The waxy crude oil pour points were measured with a Herzog Automatic Pour Point Analyser Unit MP852 (Walter Herzog GmbH, Germany) according to the ASTM D97 standard method ('Standard Test Method for Pour Point of Petroleum Products'). The specimen was examined at intervals of 3 °C from 9 °C above the anticipated pour-point temperature. The pour point was the lowest temperature at which specimen movement was observed when the tube was held horizontally for 5 s. Its repeatability is ±3 °C.

2.4. Rheology

Viscosity measurements were conducted using a controlled-stress rheometer with the coaxial cylinder test system Z41Ti (RS150 from HAAKE Corp., Germany) equipped with a programmable thermal bath (HAAKE F8/C35). The oil specimen prepared in section 2.1 was loaded into the coaxial cylinder system preheated to the filling temperature, and then cooled to the measurement temperature at the cooling rate of 0.5 °C min^{-1}, and finally measured after being held isothermally for 20 min.

2.5. Fractal box-counting method

In many fields the fractal theory is an effective means for the fast direct characterization of projection morphologies and structures from molecular scale to the large-scale universe,

and it provides new conceptual insights. For example, cloud boundaries, mountain skylines, coastlines and many others natural objects have forms much better described in fractal terms than by the straight lines and smooth curves of classical geometry. The fractal dimension is independent of the measurement yardsticks over a given range of length scales. By using this simple parameter, the high complexity of projection morphologies of many natural objects can be described rather than having to use many parameters [26, 28, 29].

The wax crystals that naturally grow in crude oils have typical highly nonlinear and irregular characteristics. On microscopic examination, their morphologies and structures geometrically show some self-similarity to a certain degree and could most likely satisfy being considered 'fractal' for further investigation. Wax crystal images are shown in the subsequent sections.

The box-counting method is very suitable for image-based fractal measurements [26]. As long as the measured objects are two-dimensional microstructures such as irregular curves, aggregates and networks, their dimensions can be estimated using this method [26]. In practice, it has been successfully used in many other fields [26, 28, 30–33] to determine whether the objects are fractal. Since the wax crystal micrographs have an analogy with the images investigated in the literature [26, 28, 32, 33], this study could also use this method.

According to the Hausdorff measure, when a geometric object is covered by a measuring box with size δ, and if the required box number N could satisfy the power law,

$$N(\delta) \propto \delta^{-D}, \tag{5}$$

it can be considered as fractal with a fractal box dimension, D [26, 29]. If δ is transformed into $\alpha\delta$ in terms of scaling, (5) is rewritten as

$$N(\alpha\delta) \propto \alpha^{-D}\delta^{-D} \propto \alpha^{-D}N(\delta). \tag{6}$$

This shows that $N(\delta)$ has self-similarity and scaling independence.

For convenience of explanation, (5) is rewritten as

$$\log N = \log C - D \log \delta \tag{7}$$

where C is a constant.

The algorithm of the box-counting method is described as follows [26]: (a) divide an image into squares with size δ_i, where $i = 1, 2, \ldots, k$; (b) count the number of boxes N_i that intercept with the measured object; (c) calculate the data sequences $\{\log \delta_i\}$ and $\{\log N_i\}$; (d) use (7) estimate the fractal box dimension by a least squares regression method.

2.6. Reliability evaluation of fractal box dimension measurement [26]

There are the F-distribution and t-distribution methods commonly used to test the regression significance of (7) in statistics. Substantially, when used in this situation, the two methods are equivalent. In this work the t-test is used to evaluate the reliability of fractal box dimension measurement based on microscopic images.

In the t-distribution method, assume that D' is the estimated value of the slope D:

$$D' = \frac{l_{\log\delta \log N}}{l_{\log\delta \log\delta}} \tag{8}$$

where $l_{\log\delta\log\delta}$ is the square sum of the difference between $\log\delta_i$ and its mean $\overline{\log\delta_i}$, and $l_{\log\delta\log N}$ is the product sum of the difference between the two variable specimen observations ($\log\delta_i$ and $\log N_i$) and their individual mean value. The subscript index i ranges from 1 to n

(the number of different box sizes). Let σ_D be the standard deviation of the slope D specimen. The t-statistics is

$$t = \frac{(D' - D)}{\sigma_D} \sim t(n-2). \tag{9}$$

The hypothesis is generally stated as H: $D = 0$, which is a presumption that there is no correlation between $\log\delta$ and $\log N$. Let SSD be the residual sum of squares which is caused by the random error. The equation (9) is changed into:

$$t = \frac{D'}{\sigma_D} = D'\sqrt{\frac{(n-2)l_{\log\delta\log\delta}}{SSD}} \sim t(n-2). \tag{10}$$

If $|t| \geqslant t_{\alpha/2}(n-2)$, the hypothesis should be rejected and linear regression is considered to be significant at the level of α. If not, it shows that $\log N$ is independent of $\log\delta$.

2.7. Optical microscopy and fractal box dimension extraction

Optical microscopy is ideally suited for the study of suspensions containing solid particles in the micrometre-size range which associate to form aggregates of several micrometres in diameter, and provide information concerning particle aggregation kinetics, floc compactness, and fractal properties [30]. The wax crystals or clusters in waxy crude oils can meet this condition.

In this work, waxy crude oil specimens were observed by a Nikon OPTIPHOT2-POL polarizing microscope, which was configured with a Linkam PE60 Peltier thermal stage in the temperature range −20 to 90 °C with a control stability of ±0.1 °C. Wax crystals were photographed with a CoolSNAP 3.3M digital CCD colour camera (Roper Scientific Inc., USA) connected to a computer. Images were processed and analysed with *ImageJ* (from Wayne Rasband, at the Research Services Branch, National Institute of Mental Health, USA). The fractal box dimensions were extracted from the images with the Fractal Box Count plug-in of the software.

The sealed vessel filled with oil specimen prepared in section 2.1 was put into the thermal bath serving the rheometer, and cooled along with the oil in the rheometer cup at the same cooling rate. When the measurement temperature was reached, the specimen was held isothermally for 20 min. Then it was quickly spread on a glass slide on the preheated thermal stage of the microscope for observation of waxy crystals and for snapshots of their micrographs with time.

The detailed image process procedures are described as follows: (a) carry out the enhancement to the wax crystal images to process and to remove any noise spots; (b) extract the wax crystal or aggregate boundary; (c) statistically analyse the boundary fractal box dimensions.

It can be observed from the visual fields of the microscope that the wax crystals or clusters are dispersed in a two-dimensional projection plane, lacking entirety and continuity. The morphologies and structures of wax crystals, whether in the virgin crude oils or in the PPD-beneficiated ones, are extremely intricate. Therefore, the most practical approach is still as far as possible to obtain more high-resolution micrographs of each crude oil specimen, in an attempt to statistically estimate or reflect the real microstructures of crude oils. Generally, about ten high-quality micrographs (2048 × 1536 pixels) were saved for processing and analysis, whose averaged fractal dimension was used to improve the precision.

For the stochastic micrographs, a statistical comparison method is used for algorithm accuracy examination as follows: (a) photograph ten high-quality microscopic images (2048 × 1536 pixels) for each crude oil specimen; (b) extract the boundary box dimension of wax crystals using the box-counting method and simultaneously carry out the t-distribution test

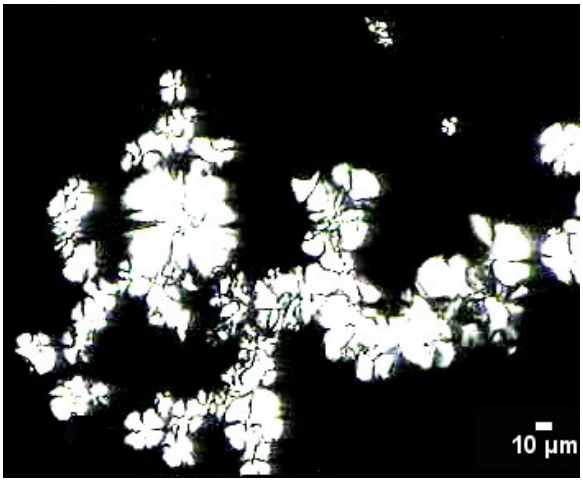

Figure 1. An image of wax crystal aggregates in a PPD-beneficiated crude oil at 2 °C cooled in quiescent condition.

Table 2. Calibration for fractal box dimension estimation.

Theoretical fractal set	Computed box dimension value	Theoretical box dimension value	Relative deviation (%)
Straight line	0.9726	1	−2.74
Cantor set	0.6607	0.6309	4.72
Koch set	1.2624	1.2618	0.05
Sierpinski gasket set	1.5532	1.583	−1.88

one by one; (c) perform the statistical analysis on the ten obtained box dimensions in terms of the indices of the average value, the standard deviation and the relative range.

By way of example, for an original image of wax crystal aggregates (figure 1, 352 × 288 pixels), after boundary extraction and binarization it is processed into a grey image (figure 2(a)). Ten different boxes with sizes ranging from 2 to 128 are taken. Each corresponding box number $N(\delta)$ is measured in accordance with the box-counting method. Then the log–log plot of the box count versus the box size is made. If this plot is assumed as a straight line, its slope is the fractal box dimension. Figure 2(b) shows the box dimension data plot. Additionally, various statistics values are separately calculated in terms of the t-test method: $l_{\log\delta\log\delta} = 3.0996$, $l_{\log\delta\log N} = 4.6955$, $D' = \frac{l_{\log\delta\log N}}{l_{\log\delta\log\delta}} = 1.5149$, $SSD = 0.0103$, $t = \frac{D'}{\sigma_D} = D'\sqrt{(n-2)\frac{l_{\log\delta\log\delta}}{SSD}} \approx 74.3298$. One can find from a t-distribution quantile table that $t_{0.01/2}(n-2) = t_{0.005}(8) = 3.3554$. For $t > t_{0.01/2}(10-2)$, one can use the confidence level of 99% to judge the $\log\delta$–$\log N(\delta)$ relation to be linear, and namely to consider the data of $N(\delta)$ and δ in agreement with the power law. So this wax crystal structure is determined as fractal, and D is its boundary box dimension.

The software *ImageJ* had been calibrated via four classical theoretical fractal sets before estimating the boundary box dimension of the wax crystals. The calibrations are listed in table 2, which indicates that the computation has a certain satisfactory veracity and reliability.

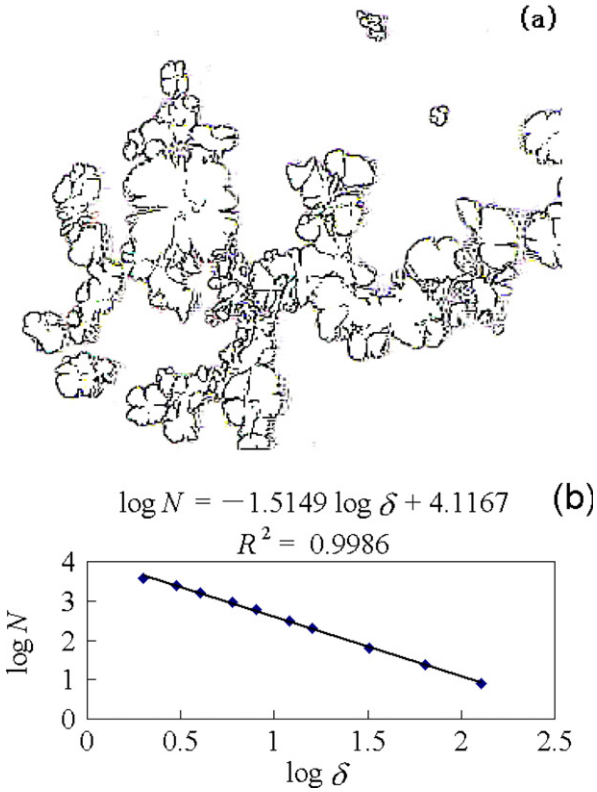

Figure 2. (a) The wax crystal aggregate boundary extracted from figure 1. (b) The box count N versus the box size δ of the wax crystal aggregate boundary measured according to the box-counting method, in a log–log plot. The box dimension, 1.5149, is obtained from the slope of the line.

3. Results and discussion

3.1. Comparison of morphologies and structures of wax crystals or aggregates in waxy crude oils beneficiated with and without a PPD

The wax crystals or aggregates statically grow in the environment of crude oils. Figure 3 is an example of the micrograph of wax crystals in virgin oil A (taken at 20 °C). It shows that the waxy crystals are quasi-sphere-shaped particles and have a corresponding homogeneous size distribution. At the same time, the wax crystals exist in an indistinctive state of coacervation. Due to the relatively high degree of dispersity of the particles, the system of a virgin waxy crude oil has a high surface energy. Once intense cooling or high shearing has been imposed, the wax crystals easily tend to interconnect into a three-dimensional network structure, which could deteriorate the flow properties of the waxy crude oil.

In contrast, figure 4 displays the wax crystal aggregates in oil A beneficiated with a PPD (taken at 20 °C). Compared with figure 3, the single wax crystals here become bigger and have tended to aggregate as masses or clusters, which increases the zone unoccupied by the particles. Furthermore, because forming a three-dimensional network structure needs more wax precipitated, the direct result is that the low-temperature flow properties of oil A are improved. For instance, the gel point of oil A beneficiated with a PPD was 2 °C, 10 °C lower than that of virgin oil A, 12 °C, cooled and measured quiescently from the heat treatment temperature of

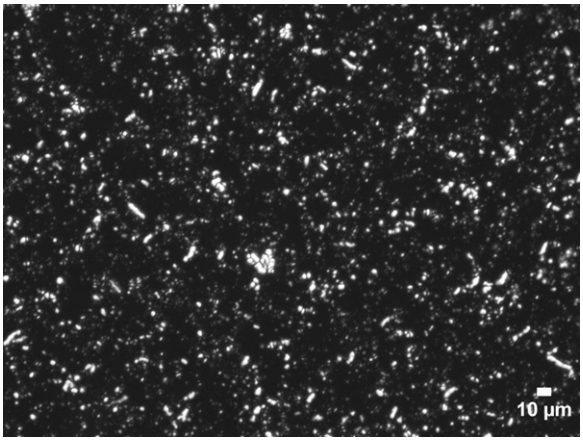

Figure 3. Optical micrograph of wax crystals in virgin oil A taken at 20 °C.

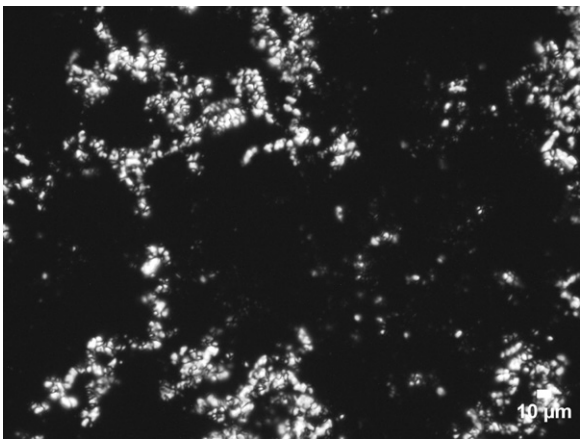

Figure 4. Optical micrograph of wax crystal aggregates in PPD-beneficiated oil A taken at 20 °C.

55 °C. This investigation confirms that the gel structure strength may be related to the types of the wax crystal morphology and structure. The structure strength of wax crystals in figure 3 could be stronger than that of wax aggregates in figure 4. For better understanding, by way of illustration there are more similar comparison micrographs (figures 5 and 6 for oil A, figures 7–10 for oil B).

As seen from the two-dimensional micrographs, along with decreasing oil temperature, the wax crystals tend to grow in more and more intricate morphologies and structures. In the virgin waxy crude oils at high temperatures, because of the small wax precipitation amount, the wax crystals are undeveloped. It is found that the quite tiny particles disperse uniformly, the intergranular porosity is rather large and the structure bonding is very weak. As the oil temperature is reduced, the wax crystals separate out more and more, and tend to interlock together and to form a three-dimensional network, which may entrap the liquid oil and cause the waxy crude oil to gel.

In the PPD-beneficiated waxy crude oils at high temperatures, aggregates or clusters agglomerated by wax crystal particles are most often seen. The inter-aggregate porosity is

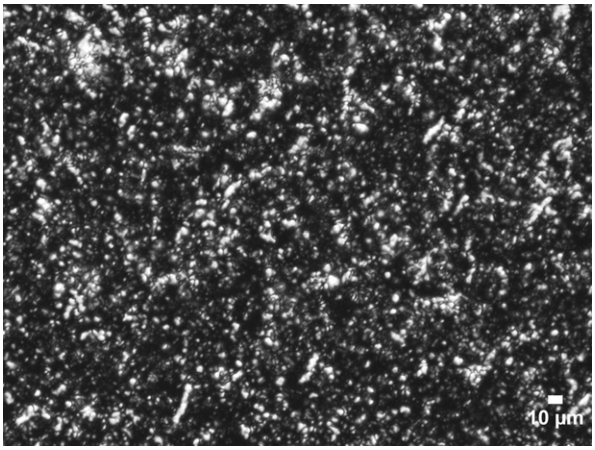

Figure 5. Optical micrograph of wax crystals in virgin oil A taken at 6 °C.

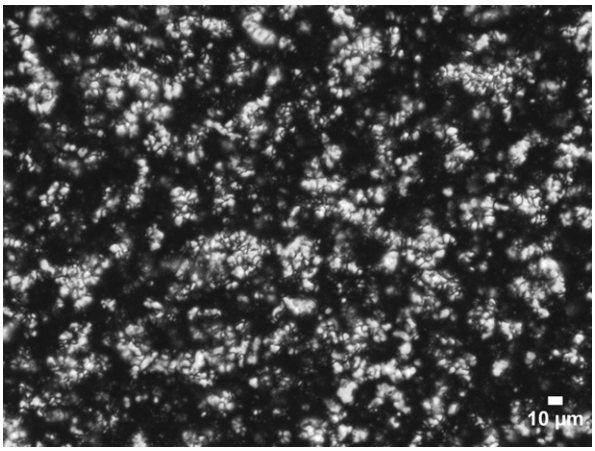

Figure 6. Optical micrograph of wax crystal aggregates in PPD-beneficiated oil A taken at 6 °C.

rather large and the structure bonding is weak. Moreover, when the crude oil temperature is lowered, not only do the individual wax crystals become bigger, but also their aggregates become more intricate in morphology and structure. There are increasingly more wax crystal aggregates with a petal shape. The degree of overlapping and the compactness between aggregates are enlarged, and the cross-linking is strengthened. When the oil is cooled further to a temperature below its pour point, the clusters could be interconnected into a three-dimensional network. Thus all liquid oil may be entrapped, which finally makes the crude oil gel. In general, due to the complex comprehensive physical and chemical effects, the flow parameters such as the pour point, gel point and viscosity of a waxy crude oil could be sharply depressed after adding enough amount of suitable PPD.

By this token, wax crystals in crude oils naturally have typical nonlinear characteristics and could most likely satisfy being considered 'fractal'. So it is possible that they may be reasonably determined as fractal subjects for investigation.

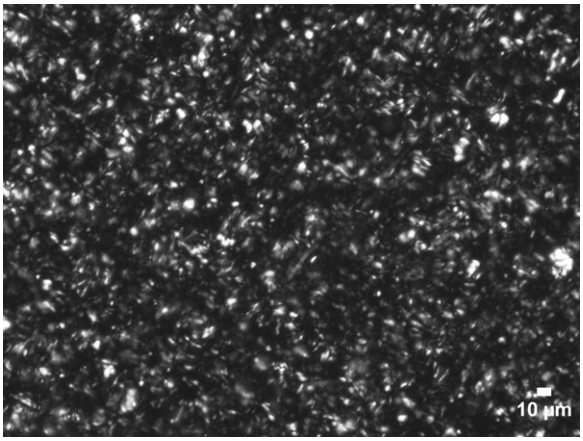

Figure 7. Optical micrograph of wax crystals in virgin oil B taken at 16 °C.

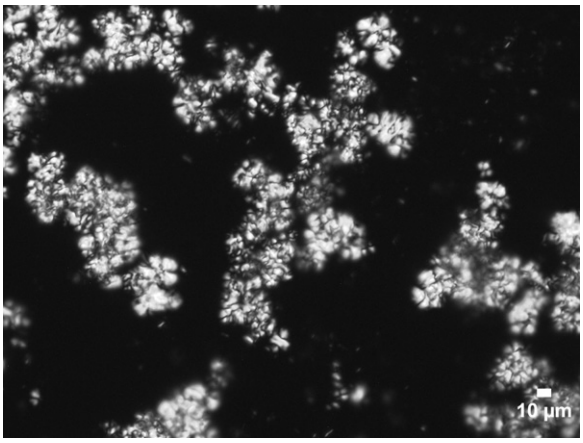

Figure 8. Optical micrograph of wax crystal aggregates in PPD-beneficiated oil B taken at 16 °C.

3.2. Boundary box dimension comparison of wax crystal structures of different visual fields of a specimen

In this study the significance of the fractal dimension lies in quantifying the highly nonlinear characteristics of the wax crystal morphology and structure. For a crude oil specimen on the microscope stage, the wax crystals or clusters of different visual fields are dispersed stochastically in appearance, but their fractal dimensions should be identical within a certain error range. Thus, this parameter could stably and effectively describe the overall structural characteristics of wax crystals growing under the same conditions.

The paper [32] established that micrographs with sufficiently large number of pixels (at least 500 pixels) are necessary to obtain a straight line of box count versus box size in log–log coordinates. Therefore, in this investigation, for oils A, B and C at every measurement temperature, ten high-quality micrographs (2048 × 1536 pixels) of wax crystals or aggregates in different visual fields of each specimen were obtained and saved. Then, the fractal box dimension of the wax crystal boundary from every image was measured using the box-counting method.

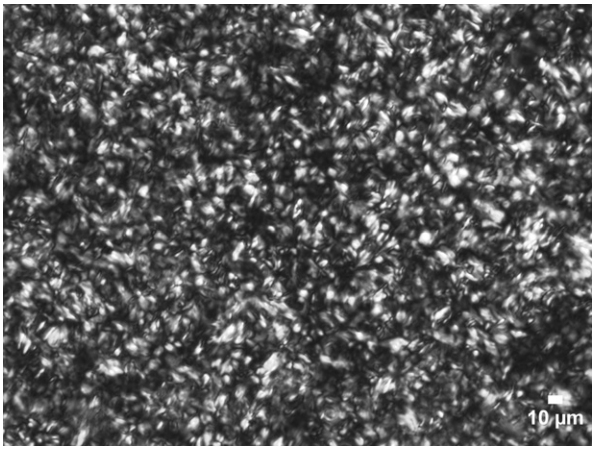

Figure 9. Optical micrograph of wax crystals in virgin oil B taken at 4 °C.

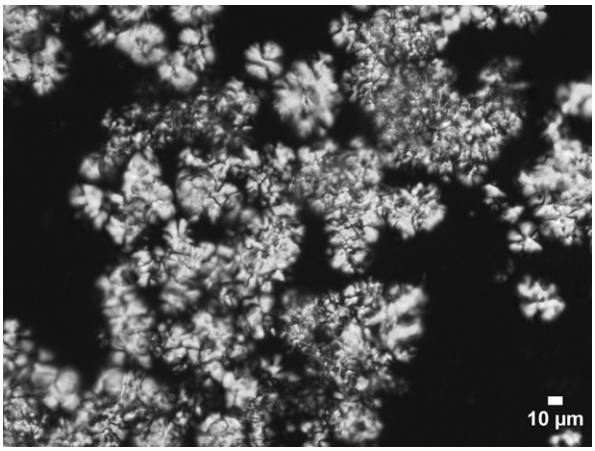

Figure 10. Optical micrograph of wax crystal aggregates in PPD-beneficiated oil B taken at 4 °C.

For instance, for oil A and oil B treated with and without a PPD, figures 11 and 12 show the boundary box dimension data distribution from the ten micrographs of different visual fields at each measurement temperature. Tables 3–6 list the deviation evaluation data respectively for oils A and B. The following aspects can be seen. The maximum and the minimum of the relative range, which is the percentage difference between the smallest and the largest values compared with the average one, are 9.97% and 1.88% respectively. This index can conservatively reflect the dispersion degree of the specimen data in relation to one another. Moreover, the standard deviations fluctuate between the maximum value of 0.0549 and the minimum of 0.0107. This shows that for each group of box dimension data at every measurement temperature, the rate of divergence is small and there is only little fluctuation existing around the average value. All the information demonstrates that the boundary box dimensions of wax crystals or aggregates in different visual fields of each specimen have substantial agreement. In other words, it is feasible to use the boundary box dimension for wholly characterizing the wax crystal morphology and structure.

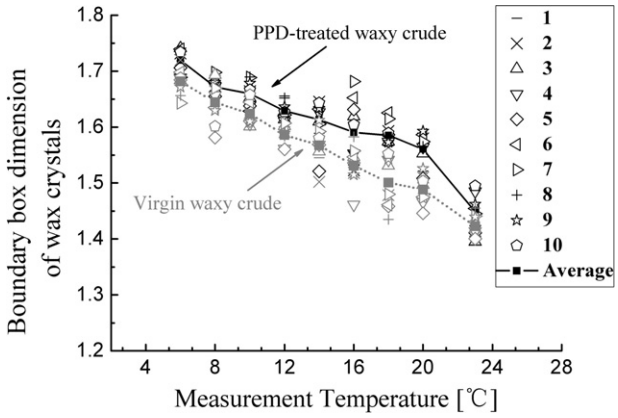

Figure 11. Measurement temperature variation of boundary box dimensions of wax crystals in oil A beneficiated with and without a PPD. In the legend area the arabic numerals from 1 to 10 and the 'average' represent the ten fractal box dimension values extracted from the ten wax crystal micrographs of ten visual fields, and their average value at each measurement temperature respectively. The black legends and solid line denote the values of virgin oil, and the grey ones and dotted line denote those of PPD-beneficiated oil.

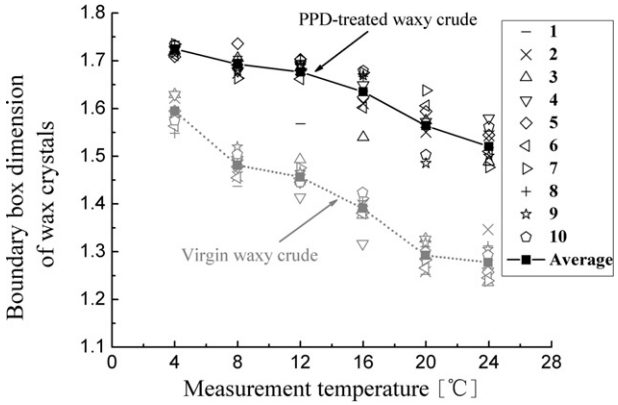

Figure 12. Measurement temperature variation of boundary box dimensions of wax crystals in oil B beneficiated with and without a PPD. Please refer to figure 11 for the legend captions.

In the regression analysis of the fractal measurement, all the correlation coefficient values are larger than 0.99. This indicates a good linear correlation between the logarithmic values of the box count and the box size. However, sometimes a test of linear hypothesis is still needed to gain insight as to at which level the hypothesis is true [26]. The bigger the absolute value of the t-statistics is, the more it supports the alternative hypothesis; namely, the more convincingly wax crystals are assumed to be fractal. Therefore, the t value may be taken as a measure of linear correlativity between the logarithms of the box size and the box count. According to this principle, tests of hypothesis on linear correlation are made for every boundary fractal dimension measurement. For instance, the statistic data of oils A and B treated with and without a PPD are demonstrated in tables 3–6 respectively. It can be seen that the minimum absolute value of the t-statistics is 29.568, which is much higher than the values of the corresponding t-quantiles with the maximum of 3.4995. So there is a confidence level of above 99% to think

Table 3. Statistical analysis of boundary box dimensions of wax crystals in virgin oil A.

Different visual fields	Absolute t statistics of box dimension of wax crystal boundary at different temperatures ($\|t\| > t_{0.01/2}(10-2) = 3.3554$)								
	23 °C	20 °C	18 °C	16 °C	14 °C	12 °C	10 °C	8 °C	6 °C
1	71.411	54.971	58.617	42.731	48.701	49.931	75.172	54.329	52.051
2	80.268	53.507	49.931	36.377	55.214	49.259	52.328	51.990	53.762
3	83.545	48.677	54.589	39.422	53.539	54.231	56.125	52.533	51.915
4	73.052	47.238	55.427	33.589	52.447	42.353	54.900	53.325	50.905
5	69.513	45.170	53.832	29.568	58.492	45.373	52.778	60.102	52.663
6	69.668	47.700	52.031	34.049	56.132	45.433	55.541	54.318	53.492
7	97.501	49.871	51.092	55.285	52.452	48.755	51.404	52.496	52.549
8	82.892	51.054	52.431	56.115	84.766	44.134	51.647	52.630	51.654
9	75.483	49.108	53.973	54.242	56.141	45.540	52.202	54.738	51.586
10	—	52.952	54.985	—	51.473	—	53.682	52.262	52.044
Deviation evaluation of box dimensions of micrographs at each measurement temperature									
Average[a]	1.4227	1.4884	1.5009	1.5312	1.5675	1.5862	1.6238	1.6444	1.6818
Standard deviation[b]	0.0207	0.0239	0.0446	0.0342	0.0295	0.0159	0.0222	0.0412	0.0213
Relative range (%)[c]	4.55	5.38	7.84	7.92	7.02	2.93	3.63	6.87	4.57

[a] Average $D_{\mathrm{a}} = \frac{\sum_{i=1}^{n}(D_i)}{n}$;

[b] Standard deviation $= \sqrt{\frac{n\sum_{i=1}^{n}(D_i - D_{\mathrm{a}})^2 - (\sum_{i=1}^{n}|D_i - D_{\mathrm{a}}|^2)}{n(n-1)}}$;

[c] Relative range (%) $= \frac{\max D_i - \min D_i}{D_{\mathrm{a}}} \times 100\%$, where D_i is the box dimension of wax crystals in a micrograph taken at the same measurement temperature and $i = 1, 2, 3, \ldots, 10$.

Table 4. Statistical analysis of boundary box dimensions of wax crystal clusters in PPD-beneficiated oil A.

Different visual fields	Absolute t statistics of box dimensions of wax crystal boundary at different temperatures ($\|t\| > t_{0.01/2}(13-2) = 3.1058$)								
	23 °C	20 °C	18 °C	16 °C	14 °C	12 °C	10 °C	8 °C	6 °C
1	99.751	122.900	89.672	98.693	61.531	62.252	54.472	50.742	60.300
2	80.268	171.031	79.822	79.762	66.841	48.319	60.912	56.935	62.394
3	53.225	114.033	83.363	89.329	71.656	56.241	56.091	61.983	68.243
4	73.255	112.543	78.548	81.424	74.947	55.511	53.432	58.951	55.294
5	47.975	78.987	72.286	90.707	61.601	55.582	66.962	54.063	62.916
6	54.290	285.093	73.804	98.148	64.040	52.824	61.403	56.075	65.166
7	66.340	101.320	74.804	93.474	73.460	52.592	65.462	65.422	61.952
8	57.567	131.840	66.404	76.098	81.643	52.337	62.954	56.765	66.689
9	59.600	394.490	113.376	72.703	59.360	60.865	63.468	62.324	67.785
10	68.948	—	77.867	82.121	65.579	59.509	65.834	58.231	69.545
Deviation evaluation of box dimensions of micrographs at each measurement temperature									
Average	1.4491	1.5606	1.5854	1.5905	1.6136	1.6290	1.6596	1.6719	1.7194
Standard deviation	0.0344	0.0286	0.0215	0.0549	0.0370	0.0151	0.0216	0.0140	0.0206
Relative range (%)	6.89	5.38	4.36	9.97	7.73	2.75	3.69	2.57	3.05

of $N_\delta(F)$ being consistent with δ in terms of the power law relation, which states clearly that the wax crystals or clusters are fractal.

Table 5. Statistical analysis of boundary box dimensions of wax crystals in virgin oil B.

Different visual fields	Absolute t statistics of box dimensions of wax crystal boundary at different temperatures ($\|t\| > t_{0.01/2}(9-2) = 3.4995$)					
	24 °C	20 °C	16 °C	12 °C	8 °C	4 °C
1	46.214	36.646	85.763	117.794	98.627	68.641
2	62.642	38.297	74.335	98.848	106.446	73.776
3	36.410	53.534	68.135	121.349	127.092	68.445
4	43.135	52.876	51.169	80.864	108.049	68.194
5	38.203	38.267	73.347	79.548	105.011	69.073
6	41.053	38.743	66.859	104.807	106.179	82.726
7	35.634	44.087	79.529	122.794	115.027	77.793
8	51.580	45.824	84.982	120.306	103.271	88.905
9	50.698	49.052	76.287	124.032	108.691	75.019
10	44.804	46.555	86.211	104.418	104.365	75.339
Deviation evaluation of box dimensions of micrographs at each measurement temperature						
Average	1.2776	1.2926	1.3910	1.4566	1.4813	1.5947
Standard deviation	0.0365	0.0278	0.0308	0.0212	0.0252	0.0296
Relative range (%)	8.68	5.72	7.70	5.39	5.57	5.10

Table 6. Statistical analysis of boundary box dimensions of wax crystal clusters in PPD-beneficiated oil B.

Different visual fields	Absolute t statistics of box dimensions of wax crystal boundary at different temperatures ($\|t\| > t_{0.01/2}(13-2) = 3.1058$)					
	24 °C	20 °C	16 °C	12 °C	8 °C	4 °C
1	73.125	79.486	85.542	61.026	104.115	95.644
2	67.741	102.998	83.844	77.882	428.250	73.538
3	61.265	94.562	53.177	73.405	176.205	111.021
4	65.609	108.108	63.948	78.541	158.059	118.642
5	69.717	72.908	66.984	69.617	101.994	92.042
6	72.648	86.399	59.637	86.413	100.885	92.331
7	48.620	79.854	69.785	70.216	151.286	73.527
8	65.415	67.648	94.934	82.489	196.020	110.633
9	54.681	64.378	68.323	87.456	140.855	90.965
10	65.643	79.797	69.083	85.026	157.888	72.916
Deviation evaluation of box dimensions of micrographs at each measurement temperature						
Average	1.5205	1.5642	1.6353	1.6768	1.6929	1.7248
Standard deviation	0.0355	0.0453	0.0434	0.0401	0.0211	0.0107
Relative range (%)	6.77	9.76	8.53	8.06	4.28	1.88

3.3. Variation of the average boundary box dimensions of wax crystals with the measurement temperatures

For oils A, B and C, the average boundary box dimensions of wax crystals before and after PPD treatment versus measurement temperatures are shown in figures 11–13 respectively. The average box dimension values generally increase along with decreasing measurement temperature. At high temperatures below the WAT, only a small quantity of quite tiny wax crystals in the virgin waxy crude oils separates out, and disperses homogeneously; these

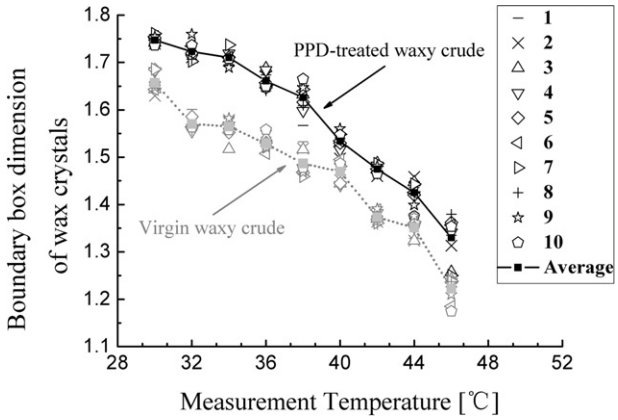

Figure 13. Measurement temperature variation of boundary box dimensions of wax crystals in oil C beneficiated with and without a PPD. Please refer to figure 11 for the legend captions.

have small fractal box dimensions, which characterize their quite simple morphologies and structures. When the oil temperature is lowered, the precipitated wax amount is increased, and the grain size is augmented; simultaneously the weak aggregation of wax crystals may be observed. As a result, the corresponding box dimensions have increased. For example, for virgin oil B the boundary box dimensions of wax crystals change from 1.2776 ± 0.0365 at 24 °C to 1.5947 ± 0.0296 at 4 °C.

Similarly, the average boundary box dimensions of wax crystal aggregates increase with decreasing oil temperature for PPD-beneficiated crude oils. For instance, for PPD-beneficiated oil B the boundary box dimensions of wax crystal clusters vary from 1.5205 ± 0.0355 at 24 °C to 1.7248 ± 0.0107 at 4 °C.

Besides that, after the PPD beneficiation at each given temperature the average boundary box dimension of wax crystals becomes distinctly larger than that of the virgin oil. In a virgin waxy crude oil the wax crystals disperse uniformly in grain size, and their corresponding fractal dimension is small, which shows the morphology and structure are simple. In contrast, after the PPD beneficiation the wax crystals assemble as aggregates or masses, and their fractal dimensions become bigger, which suggests that their morphology and structure are relatively intricate. For oil B as an example, the average fractal dimensions of wax crystals rise by the amplitudes of 0.2429 at 24 °C and 0.1301 at 4 °C after the PPD beneficiation.

Therefore, the parameter of the fractal dimension may effectively distinguish the nonlinear and irregular characteristics of microstructure of a waxy crude oil.

Through further observation of figures 11–13, it is discovered that one may develop a new approach to quantitatively evaluating the PPD beneficiation effect on waxy crude oils to a certain extent from the microscopic point of view. Maybe this needs to use the variation amplitude of the fractal dimension in combination with some parameters of the crude oil composition and some wax crystallization parameters. For instance, after the same heat treatment at 65 °C the pour point of virgin oil C is 35 °C (32 °C for the gel point), and that of oil C treated with a 200 mg kg^{-1} dosage of PPD is reduced to 25 °C (22 °C for the gel point), namely a drop of 10 °C; the apparent viscosity of virgin oil C is 1547.5 mPa s, and the corresponding value is reduced to 71.7 mPa s after the PPD treatment, namely a viscosity reduction of 95.4%, at the survey temperature 30 °C and under the shear rate 20 s^{-1}. The apparent viscosity reduction versus the measurement temperature for oil C under imposed three shear rates is plotted in figure 14. In comparison with the traditional evaluation methods,

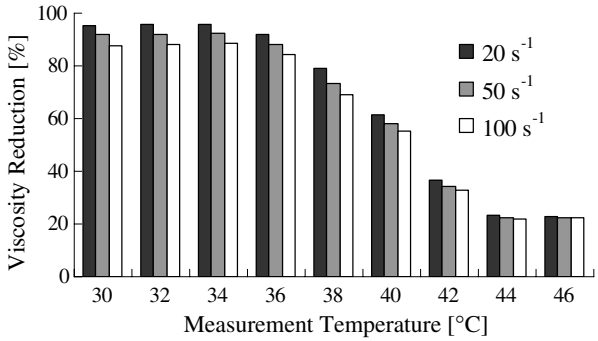

Figure 14. Viscosity reduction versus measurement temperatures for oil C before and after PPD beneficiation. The black, grey and white bars represent the apparent viscosity reduction values under the shear rates of 20, 50 and 100 s^{-1} respectively.

$$\text{Viscosity reduction } (\%) = \frac{\text{Virgin crude viscosity} - \text{PPD-beneficiated crude viscosity}}{\text{Virgin crude viscosity}} \times 100\%.$$

this novel one may be expected to assess a PPD experimental additive more quickly, more conveniently and economically. With a view to the complexity of the rheology–microstructure relation, this particular issue is indeed difficult and thus need studying thoroughly.

From the viewpoint of the measurement temperature variation of the microstructure fractal dimension, this work is basically similar to [9, 17] in terms of the waxy crude oil gels involved; however, it is a little different from [34]. It may be seen from the microscopic images reported by [34] that this is likely to lie in the great differences between wax crystal morphologies and structures of a model crude oil and an actual waxy one. For an actual waxy crude oil gel, Kané *et al* [9] calculated some fractal dimension values of three-dimensional microstructures (2.4 at 25 °C, 2.3 at 27.5 °C and 2.2 at 30 °C respectively) by using viscosity data and equation (4) [23]. For a model crude oil obtained by mixing linear and branched paraffins into a saturated hydrocarbon solvent, Vignati *et al* [34] conducted small-angle light scattering studies at temperatures between the cloud point (58 °C) and sol–gel transition (39 °C). The result showed that clusters formed by the aggregated wax solids possessed an almost constant fractal dimension of about 1.8.

Nevertheless, perhaps the paper [34] ignored the experimental phenomenon of the temperature variation of the precipitation quantity and the morphology and microstructure of wax crystals. Moreover, according to the statement of [35], at present, it is difficult to have a clear idea of the type of crystals naturally occurring in crude oils cooled below the WAT; there is no general agreement either on the shape (platelet or needle) or the average size (from nanometres to several microns). And the difficulties may be related to many factors, such as the specimen preparation method, the observation technique and the solution molecular composition. It is really hard to expect completely consistent observations of the wax crystal morphologies between the crude oil and the model one. But, just like the way used in [34], it is somewhat preferable to investigate the effect of a single factor on the wax crystal morphology and structure via experiments on the model crude oil.

3.4. Comparison with the calculated actual fractal dimension obtained using the indirect approach

A comparison was made between the fractal dimensions obtained using the direct image-based approach and the indirect one based on the viscosity data. According to the procedures in [9],

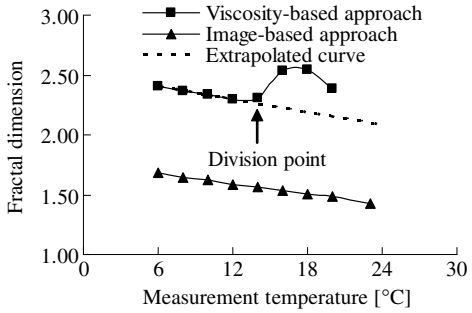

Figure 15. Comparison between the fractal dimensions obtained using the direct image-based approach and the indirect viscosity-based one for virgin oil A. The extrapolated curve is made based on the calculated fractal dimensions at temperatures below the 'division point'.

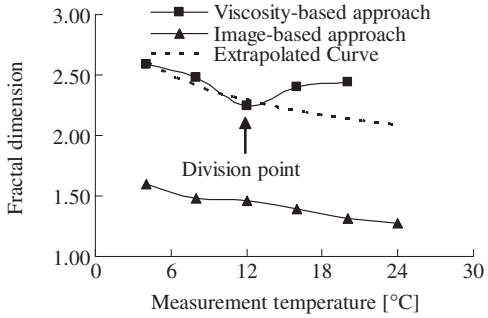

Figure 16. Comparison between the fractal dimensions obtained using the direct image-based approach and the indirect viscosity-based one for virgin oil B. The extrapolated curve is made based on the calculated fractal dimensions at temperatures below the 'division point'.

the actual fractal dimension of the wax crystals was calculated by taking virgin oils A and B as the examples and using equation (4). All the fractal dimension data of virgin oils A and B are compared in figures 15 and 16. The two figures clearly show that the variation of the actual fractal dimensions with the temperatures below the 'division point' (nearby the gel point) is consistent with that of [9]. However, at temperatures above the 'division point' the viscosity-based fractal dimension values obviously fail in characterizing the microstructure of wax crystals in crude oils. This point is not discussed in [9], and the analysis is limited to the crude oil gel below the gelation temperature. Judging empirically by the wax precipitation characteristics in waxy crude oils, the fractal dimensions above the 'division point' may follow the extrapolated curve based on those data at temperatures below the 'division point', as shown by the dashed curves in figures 15 and 16. The relation between the fractal dimension and temperature obtained using the image-based approach is in reasonable agreement with that presented by the extrapolated curve. From microscopic observations this implies that the fractal dimension is associated with the growth process of the wax crystals in crude oils.

Similar to the situation of [30, 32], it should be mentioned that the main drawback of all the image-based methods is that the image is the two-dimensional projection of the actual morphology and structure. Therefore, the fractal dimensions measured by image analysis techniques are intrinsically lower than the actual values for three-dimensional objects. However, as mentioned in [30], the paper [36] has proposed that the fractal dimension values measured from the two-dimensional projection concur with the real values of D, and that

the boundary fractal dimension of the two-dimensional aggregates is a nontrivial continuously varying function of D.

4. Conclusions

This work uses the direct fractal approach based on micrograph analyses for characterizing the morphology and structure of wax crystals in crude oils. With this approach, the microstructure data can be obtained independently. It is in contrast to other studies [9, 17, 18] where indirect approaches were used to deduce the microscopic properties of waxy crude oils.

The box-counting method is applied to the image-based characterization of microstructures of three waxy crude oils before and after PPD beneficiation. It is shown that the boundary box dimensions from micrographs of different visual fields of a specimen are almost identical, with the maximum and minimum relative ranges being 9.97% and 1.88% respectively, and with the standard deviation ranging from 0.0549 to 0.0107. The box dimension data at each measurement temperature from different visual fields have a small fluctuation around the average value. The results also show that a larger boundary fractal dimension represents a higher complexity of the wax crystal morphology. The wax crystal boundary box dimensions are found to increase with decreasing oil temperature for each waxy crude oil. After the PPD beneficiation, the fractal dimension at each given measurement temperature increases noticeably.

Measurement reliability of every box dimension is evaluated via the t-distribution test of hypothesis on linear regression at the significance level of 0.01. All the listed absolute t-statistics with the minimum of 29.568 are much higher than the corresponding t-quantiles with the maximum of 3.4995, which denotes high linear regression significance and represents a confidence level of 99% in considering wax crystal microstructures as fractal.

Thus, these findings verify that the wax crystal microstructures in waxy crude oils can be characterized by fractal dimensions. This helps in making a new probe into the rheology–microstructure relationship. An extensive research on this correlation will be published separately.

Acknowledgments

This work is financially supported from the key project (Grant No. 104118) for Science and Technology Research of the China Ministry of Education. W Rasband (the Research Services Branch, National Institute of Mental Health, USA) is greatly acknowledged for developing and maintaining the software *ImageJ*, and so are the authors of the plug-in of Fractal box count for contributing it. Moreover, it is our pleasure to thank Dr Lei Hou, Dr Shanpeng Han and Mr Haifeng Wang for their assistance with the experiments reported in this paper.

References

[1] Agarwal K M, Purohit R C, Surianarayanan M, Joshi G C and Krishna R 1989 *Fuel* **68** 937
[2] Rønningsen H P, Bjørndal B, Hansen A B and Pedersen W B 1991 *Energy Fuels* **5** 895
[3] Lakshmi D S, Purohit R C, Srivastava S P, Nautiyal S P, Tiwari G B, Rama Krishna M, Venkateswara Rao M and Bhagvanth Rao M 1997 *Pet. Sci. Technol.* **15** 685
[4] Chanda D, Sarmah A, Borthakur, Rao K V and Subrahmanyam B 1998 *Fuel* **77** 1163
[5] Cazaux G, Barre L and Brucy F 1998 *SPE Annual Technical Conf. and Exhibition (New Orleans, USA, Sept. 1998)* (*SPE* vol 49213) p 729
[6] Magri N F and Kalpakci B 1999 *AIChE Spring Nat. Mtg (Houston, USA, March 1999)* Paper No 60e
[7] Wardhaugh L T and Boger D V 1991 *AIChE J.* **37** 871

[8] Zhang J, Liu Z, Zhang F, Huang Q and Yan D 1997 *ISMNP'97: Proc. 1997 Int. Symp. on Multiphase Fluid, Non-Newtonian Fluid and Physico-Chemical Fluid Flows (Beijing, China, July 1997)* ed L X Zhou and X F Li (Beijing: Int. Acad. Publ.) p 715
[9] Kané M, Djabourov M and Volle J-L 2004 *Fuel* **83** 1591
[10] Visintin R F G, Lapasin R, Vignati E, D'Antona P and Lockhart T P 2005 *Langmuir* **21** 6240
[11] Shuang K, Liang H Q and Zhang J J 2002 *J. China Univ. Pet. (Edition of Natural Science)* **26** 100 (in Chinese)
[12] Shuang K and Wang L 2003 *Optical Technology and Image Processing for Fluids and Solids Diagnostics (Beijing, China, 2002)* (*Proc. SPIE* vol 5058) ed G X Shen, S S Cha, F-P Chiang and C R Mercer (Bellingham, WA: SPIE) p 367
[13] Ferris S W and Cowles H C 1945 *Ind. Eng. Chem.* **37** 1054
[14] Chang C, Boger D V and Nguyen Q D 2000 *SPE J.* **5** 148
[15] Létoffé J M, Claudy P, Kok M V, Garcin M and Volle J L 1995 *Fuel* **74** 810
[16] Hénaut I, Vincké O and Brucy F 1999 *SPE Annual Technical Conf. and Exhibition (Houston, USA, Oct. 1999)* (*SPE* vol 56771) p 349
[17] Lorge O, Djabourov M and Brucy F 1997 *Rev. Inst. Français Pétrole* **52** 235
[18] Lopes da Silva J A and Coutinho J A P 2004 *Rheol. Acta* **43** 433
[19] Buscall R, Mills P D A, Goodwin J W and Lawson D W 1988 *J. Chem. Soc. Faraday Trans.* I **84** 4249
[20] Shih W H, Shih W Y, Kim S I, Lin J and Aksay I A 1990 *Phys. Rev.* A **42** 4772
[21] Wu H and Morbidelli M 2001 *Langmuir* **17** 1030
[22] Uriev N B and Ladyzhinsky I Y 1996 *Colloid Surf.* A **108** 1
[23] Krieger I M 1972 *Adv. Colloid Interface Sci.* **3** 111
[24] Snabre P and Mills P J 1996 *J. Physique* **6** 1811
[25] Wessel R and Ball R C 1992 *Phys. Rev.* A **46** R3008
[26] Li J M, Lü L, Lai M O and Ralph B 2003 *Imaged-Based Fractal Description of Microstructures* (Boston, MA: Kluwer–Academic)
[27] Chen J, Zhang J J and Li H Y 2004 *Thermochim. Acta* **410** 23
[28] Helalizadeh A, Müller-Steinhagen H and Jamialahmadi M 2006 *Chem. Eng. Sci.* **61** 2069
[29] Chu W Y, Su Y J, Gao K W, He J Y, Li J X and Qiao L J 2004 *Fractal in Material Science* (Beijing: Chemical Industry Press) (in Chinese)
[30] Bower C, Washington C and Purewal T S 1997 *Colloids Surf.* A **127** 105
[31] Akiyama T, Iguchi T, Aoki K and Nishimoto K 1998 *Powder Technol.* **97** 63
[32] Le Coënt A L, Rivoire A, Briancon S and Lieto J 2005 *Powder Technol.* **152** 62
[33] Dathe A and Thullner M 2005 *Geoderma* **129** 279
[34] Vignati E, Piazza R, Visintin R F G, Lapasin R, D'Antona P and Lockhart T P 2005 *J. Phys.: Condens. Matter* **17** S3651
[35] Kané M, Djabourov M, Volle J-L, Lechaire J-P and Frebourg G 2003 *Fuel* **82** 127
[36] Jullien R and Thouy R 1994 *Phys. Rev.* E **50** 3878